Mixed-surface, Lipid-tethered Quantum Dots for Targeting Cells and Tissues

Yanjie Zhang[a], *Amanda Haage*[d], *Elizabeth M. Whitley*[c], *Ian C. Schneider*,[a,b] *and Aaron R. Clapp*[a]*

[*] Professor Aaron R. Clapp

Iowa State University

Department of Chemical and Biological Engineering

2114 Sweeney Hall, 50011-2230

clapp@iastate.edu

phone: (515) 294-9514

fax: (515) 294-2689

[a]Department of Chemical and Biological Engineering, Iowa State University

[b]Department of Genetics, Development and Cell Biology, Iowa State University

[c]Department of Veterinary Pathology, Iowa State University

[d]Molecular, Cellular and Developmental Interdepartmental Graduate Program, Iowa State University

Abstract

Quantum dots (QDs), with their variable luminescent properties, are rapidly transcending traditional labeling techniques in biological imaging and hold vast potential for biosensing applications. An obstacle in any biosensor development is targeted specificity. Here we report a facile procedure for creating QDs targeted to the cell membrane with the goal of cell-surface protease biosensing. This procedure generates water-soluble QDs with variable coverage of lipid functional groups. The resulting hydrophobicity is quantitatively controlled by the molar ratio of lipids per QD. Appropriate tuning of the hydrophobicity ensures solubility in common aqueous cell culture media and while providing affinity to the lipid bilayer of cell membranes. The reaction and exchange process was directly evaluated by measuring UV-vis absorption spectra associated with dithiocarbamate formation. Cell membrane binding was assessed using flow cytometry and total internal reflection fluorescence imaging with live cells, and tissue affinity was measured using histochemical staining and fluorescence imaging of frozen tissue sections. Increases in cell and tissue binding were found to be regulated by both QD hydrophobicity and surface charge, underlying the importance of QD surface properties in the optimization of both luminescence and targeting capability.

Keywords: biosensing, dithiocarbamate, lipophilic, liver binding, plasma membrane, quantitative histology

1. Introduction

For over a decade, luminescent quantum dots (QDs) have held potential to revolutionize biological imaging applications including biosensing, cell labeling and the clinical practice of pathology.[1-8] Despite many reported methods for their preparation, biocompatible QDs have been limited in these applications largely due to the shortcomings of surface ligands that confer solubility in water. The dispersion of QDs in water can be driven by either electrostatic stabilization through capping exchange with small charged ligands[1-6] or steric stabilization through coating with polymers.[7-10] Small ligands containing mono or bidentate thiol species have been used extensively to endow QDs with water-solubility. Due to relatively weak interactions with the nanocrystal surface, monothiol ligands usually cannot provide long-term colloidal stability.[11] Although the stability can be improved by using dithiol molecules, the loss of quantum yield and aggregation in biological buffers (acidic conditions and/or high salt concentrations) are persistent concerns. Polymer-coated QDs offer exceptional stability, yet their bulky size[12, 13] can limit access to confined cellular compartments *in vitro* or exclude their clearance *in vivo*. Our laboratory has overcome these challenges by developing a facile, reliable method for generating soluble, small diameter, highly luminescent QDs using dithiocarbamate (DTC) ligands.[14]

A compelling application of QDs is their use as biosensors for observing biological processes such as enzymatic activity. This creates a need for targeting QDs toward particular tissues, cells, or subcellular structures. Membrane-bound protease activity has drawn increasing attention due to its implied role in cancer invasion and metastasis.[15-17] There is an unfulfilled niche for a biosensor that can detect proteolytic activity in cell membranes for the evaluation of metastatic potential at an early stage. The optimal protease biosensor for this application exhibits bright luminescence and binds the plasma membrane with high affinity. Most current protease biosensors employ cleavage peptides which link quenched organic dyes[18-20] or variants of green fluorescence protein (GFP).[21-24] While these methods

are popular, quenched organic dyes usually lack targeting ability, and both organic dyes and GFP-based biosensors photobleach readily under continuous illumination. Variants of GFP are often used in

combination to detect cell surface protease activity through changes in Förster resonance energy transfer (FRET). However, this requires genetic expression of GFP, limiting prospects for detection *in vivo* or for use in diagnostic samples. Consequently, QDs are more desirable candidates for biosensing applications due to their broad absorption spectra, narrow and size tunable emission spectra, and superior resistance to chemical/physical degradation. Most QD-based biosensors have used antibodies to target specific proteins of interest.[25-28] Although the specificity is very high, the large size (20-50 nm) of the conjugated antibody is a frequent concern.[29, 30] Another approach is to attach a relatively small lipid to the QD directly to confer binding,[31] however the challenge is to retain aqueous solubility of the modified QD. Here we report a procedure for generating QDs which have affinity for the hydrophobic lipid-rich cell membrane while retaining aqueous solubility. The membrane localization and hydrophilicity can be achieved simultaneously by coating QDs with a lipid-like molecule, hexadecylamine (HDA), and hydrophilic ligands based on dithiocarbamate (DTC) chemistry, which was reported previously by our group.[14] The flexibility of this chemistry offers a large pool of DTC precursor candidates, allowing for flexible tuning of both hydrophobicity and surface charge of the QD.

In this study, we have developed a series of QDs with hydrophilic ligands of various magnitudes of negative charge (lysine-DTC, aminopropanediol-DTC, and cysteine-DTC) and found that the affinity to the cell membrane is differentially affected by a combination of QD hydrophobicity and charge. We subsequently tested the membrane binding affinity of the three different ligand-conjugated QD pairs using flow cytometry and total internal reflection fluorescence (TIRF) imaging on live cell cultures, and histochemical staining on fresh-frozen sections of liver tissue. We found consistent binding trends between live cells and frozen tissues that indicated that surface charge regulates the degree of enhanced binding conferred by the hydrophobic character of the QD. We intend to use these data to develop heuristics based on hydrophobicity and surface charge that can guide the design of QD-based biosensors

of cell surface protease activity.

2. Materials and Methods

2.1 Materials

Hexadecylamine (HDA, 90%), hexamethyldisilathiane ($(TMS)_2S$), trioctyl phosphine (TOP, 90%), L-lysine (≥98%), 3-amino-1,2-propanediol (97%), and diethylzinc (Zn, 52.0 wt%) were purchased from Sigma-Aldrich. Cadmium acetylacetonate ($Cd(acac)_2$) and selenium shot (Se, 99.99%) were from Strem Chemicals. Trioctyl phosphine oxide (TOPO, 98%) and *n*-hexylphosphonic acid (HPA) were obtained from Alfa Aesar. L-cysteine (≥99%) was purchased from Acros Organics. Chloroform and carbon disulfide (CS_2) were from Fisher Scientific. Mouse Embryonic Fibroblasts (MEFs) were obtained as frozen stock from Rick Horwitz (UVA). Cell media and additives including, Dulbecco's Modified Eagle's Medium (DMEM), phosphate-buffered saline (PBS), trypsin, GlutaMAX, penicillin/streptomycin and fetal bovine serum (FBS) as well as fluorescent reagents such as Alexa Fluor 488-phalloidin, DAPI, and DiD were purchased from Invitrogen. Bovine serum albumin (BSA) was from Sigma.

2.2 CdSe-ZnS Quantum Dot Synthesis

The CdSe-ZnS QDs used in this work were synthesized using the method published previously by our group.[14] In a typical procedure, a flask containing TOPO, TOP, and HDA were degased under vacuum for three hours at 140 °C before being heated to 340 °C at which cadmium ($Cd(acac)_2$) and selenium precursor (1 M TOP:Se) were rapidly injected. The temperature was immediately lowered (<100 °C) once the desired size had been reached. After annealing overnight, the excess selenium/cadmium precursor was removed by centrifugation, and the CdSe cores were kept in a mixture of toluene, butanol, and hexane. To protect the core from oxidation and improve quantum yield, the cores were then overcoated with multiple ZnS layers (3-5). During the shell synthesis, CdSe cores were added into the degassed ligand mixture (TOPO and HPA) where solvent was removed by a liquid nitrogen solvent trap,

followed by the slow addition of Zn and S precursors via a programmable syringe pump (0.4 mL/min). The synthesized CdSe-ZnS core-shell QDs were again allowed to anneal overnight at 80 °C and then stored in a mixture of solvents (toluene, hexane, and butanol).

2.3 Biphasic Ligand Exchange

The ligands used in this study were lysine (Lys), aminopropanediol (AP), and cysteine (Cys); these ligands attached to the QD surface via the DTC functional group through biphasic ligand exchange process. In short, equimolar amounts of amine precursors and CS_2 were mixed with ultrapurified water (Milli-Q System, Millipore). Purified CdSe-ZnS QDs (excess hydrophobic ligands had been removed), dissolved in chloroform were then added to the solution. The mixture was stirred vigorously for 24 hours at room temperature or until all hydrophobic QDs had been transferred to upper water phase. Excess ligands were removed using an Amicon Ultra-4 50k MWCO centrifugal filter (Millipore) and followed by passing through a PD-10 chromatography column (GE Healthcare).

Hydrophobic HDA ligands where attached to the QD surface using a similar approach. Instead of forming DTC in water, HDA-DTC was produced in chloroform by reacting with CS_2. This was mixed with water-soluble QDs and stirred overnight at room temperature. The amount of HDA-DTC per QD was varied by controlling the concentration of HDA and CS_2 in the organic phase.

2.4 Turbidity, Normalized Aqueous Concentration and Solubility Index

Turbidity index (TI), normalized aqueous concentration (NAC) and solubility index (SI) are defined as follows.

$$TI(n) = \frac{A_{660}(n) - A_{660}(1{:}0)}{A_{660}(1{:}10) - A_{660}(1{:}0)}, \quad (1)$$

where n is the QD:HDA ratio and A_{660} is the absorbance at 660nm.

$$NAC(n) = \frac{A_{585}(n) - A_{660}(n)}{A_{585}(1{:}10) - A_{660}(1{:}10)}. \quad (2)$$

$$SI(n) = \frac{NAC(n)}{TI(n)} \quad (3)$$

2.5 Cell Culture

Mouse Embryonic Fibroblasts (MEFs) were used for all live cell experiments. Cultures were maintained using DMEM with phenol red + 10% FBS, 2% GlutaMAX, and 1% penicillin/streptomycin. Cells were harvested using trypsin.

2.6 Flow Cytometry

All flow cytometry experiments used live MEF cells at approximately 500,000 cells per sample. QD solutions at 1 μM and/or DiD solutions at 10 μM with appropriate media were incubated with cells for 30 minutes and then washed twice with appropriate media. The media used for a particular sample was determined by Table 1: Lys-, Lys-HDA-, AP-, and AP-HDA-QDs were incubated in DMEM + 1 mg/ml BSA + 12 mM HEPES without phenol red and Cys- and Cys-HDA-QDs were incubated in PBS. All QDs used in each experiment had the same number of freeze/thaw cycles. The samples were stored on ice for up to 5 hours after washing to suppress endocytosis. Flow cytometry experiments were conducted at the Iowa State University flow cytometry facility. Mean fluorescence from flow cytometry was background-substracted and divided by the background-subtracted mean fluorescence of the same QD sample measured using 442 nm excitation wavelength and 605 nm emission wavelength in solution in a Fluoromax-4 dual monochromator spectrofluorometer (Horiba Jobin-Yvon) with a 0.1 s integration time.

2.7 Dynamic Light Scattering

Dynamic light scattering was performed using a Malvern Zetasizer Nano-ZS90. The intensity correlation curve was collected at 25 °C at a scattering angle of 90°.

2.8 TIRF Live Cell Imaging

All live cell time lapse imaging experiments used MEF cells at concentrations per sample conducive to obtaining single cell images, approximately 2 to 5 million cells/ml in a 35 mm dish. Cells were labeled

with 1 μM DiD for 10 minutes in DMEM with phenol red + 10% FBS, 2% GlutaMAX, and 1% penicillin/streptomycin and then suspended in DMEM lacking phenol red + 10% FBS, 2% GlutaMAX, and 1% penicillin/streptomycin, 12 mM HEPES containing Lys-QDs, or Lys-HDA-QDs. Concentrations of QDs ranged from 100 nM to 1 μM. Cells with QDs were washed 3× at low speeds in the imaging medium described above in order to eliminate unbound and/or aggregated QDs. Samples were placed in chamber slides with coverslips coated in either 30 μg/ml collagen or 10 μg/ml fibronectin. Cells were then imaged after spreading had occurred. Imaging was conducted on a Nikon TiE through-the-objective total internal reflection fluorescence (TIRF) microscope. Images were collected through ApoTIRF, 60×, 1.49 NA Nikon objective. The images were collected on an Andor iXon888 EMCCD at a frame rate > 3Hz. Consequently, 100 to 1000 frames and time intervals ranging from 90 ms to 600 ms were taken. Correlation analysis was performed as described elsewhere.[32] Briefly, small regions were selected on the cell and the following equation was used to calculate the temporal autocorrelation function, *r*, as a function of time lag, *i*, in units of frames:

$$r(i)=\frac{1}{X}\sum_{i=1}^{X}\frac{1}{N-i}\sum_{j=1}^{N-i}\frac{\left(I_j-\bar{I}_j\right)\left(I_{j+1}-\bar{I}_{j+1}\right)}{I_j\bar{I}_{j+1}}, \quad (4)$$

where X is the number of pixels in a region of interest, N is the total number of frames, I_j is the image gray value at each pixel in the region of interest at frame j, and $\bar{I}_j$ is the spatial average image gray values in the region of interest at frame j. Three sections of the lamellopodia of each cell were selected to be analyzed along with the cell body and a cell-free area. The autocorrelation function was normalized using the following equation:

$$r_{norm}(i)=r(i)/r(1). \quad (5)$$

The data was fitted to a model that describes two different populations diffusing at different rates. We hypothesize that these populations are QDs diffusing on the surface and vesicle-containing QDs

diffusing in the cell. The following equation was used for this two population diffusion model:

$$r_{norm}(i) = g_1(0)\left(1+\frac{\tau}{\tau_{d1}}\right)^{-1} + g_2(0)\left(1+\frac{\tau}{\tau_{d1}}\right)^{-1} + g_\infty, \quad (6)$$

Fits were performed using the `lsqcurvefit` function in MATLAB. Confidence intervals for parameters were calculated at the 95% level using the `nlparci` function.

2.9 Histology

Liver samples were collected from leftover hepatic tissue after a diagnostic post-mortem examination of a young dog that died after acute vehicular trauma. Liver samples were snap-frozen in Optimal Cutting Temperature (OCT) medium (Tissue-Tek) and were sectioned to 3 μm and mounted on aminoalkylsilane-coated coverslips. Samples were incubated for 30 minutes at room temperature with a mixture of individual QDs species at 0.5 M, 4',6-diamidino-2-phenylindole (DAPI), and Alexa Fluor 488-phalloidin (Invitrogen). Samples on coverslips were then washed gently three times with DMEM for Lys-QDs, Lys-HDA-QDs, AP-QDs and AP-HDA-QDs and with PBS for Cys-QDs and Cys-HDA-QDs, mounted on a glass slide using Vectashield HardSet Mounting Medium for Fluorescence (Vector Laboratories), and allowed to dry. Histologic examination was performed by a board-certified veterinary pathologist and binding of QDs to multiple cell types was evaluated subjectively using fluorescence microscopy. Prior to use in this work, hematoxylin and eosin-stained, frozen and formalin-fixed, paraffin-embedded sections of liver tissue were examined with light microscopy to determine adequacy of sectioning and processing and revealed that the liver was histologically normal. For image analysis, histological sections were imaged through a PlanFluor, 20×, 0.45 NA Nikon objective. Histologic images were collected on a Photometrics HQ^2 CCD.

2.10 Computer aided image analysis for QD-binding intensity

Image analysis to determine differential binding between cell membrane and cytoplasm was performed on at least 7 images for each slide using Adobe Photoshop CS5. Briefly, images were opened in Photoshop and an area of interest (cell border, cytoplasm, or sinusoidal background) was selected using

the “magic wand” tool, set to tolerance of 3. The area was expanded using the “similar” function, and the mean number of pixels at each intensity level (corresponding to the mean binding intensity) was recorded for five different locations on each image. The ratio of sinusoidal cell border to cytoplasmic binding was calculated by first subtracting the background binding intensity for each location and using the mean of the five locations to represent the data from an individual image. The Mann Whitney and ANOVA tests with $p = 0.05$ were used for statistical analysis.

3. Results and Discussion

Given our ability to fabricate small, highly luminescent QDs while controlling surface properties, we sought to generate mixed-surface QDs having hydrophobic moieties to enhance cell and tissue binding ability and hydrophilic moieties to enhance aqueous solubility. Optimizing these properties in combination is a critical step towards generating QDs that efficiently bind to cells and tissues. To measure the ability of our mixed surface QDs to bind cells and tissues, we first evaluated the stability and fluorescence of QDs *in vitro*, characterized the cell binding using complementary techniques of flow cytometry and high-resolution fluorescence microscopy, and measured the tissue binding using histologic techniques.

3.1 Fabrication and Characterization of Lipid-Modified Quantum Dots. As described previously, DTCs are suitable multivalent ligands for attaching amino acids and other primary amine containing molecules to CdSe-ZnS QDs, while preserving colloidal stability and desirable optical properties. The flexibility of this approach allows for tuning the balance of hydrophobicity and hydrophilicity, which impacts the affinity of these QDs for the plasma membrane of cells. Consequently, we sought to modify a hydrophobic molecule containing a primary amine using DTC chemistry. This approach was used in combination with hydrophilic ligands such as lysine, aminopropanediol, and cysteine to provide

aqueous solubility. The particular hydrophilic ligands were selected to allow different magnitudes of negative charge. These included lysine (Lys), aminopropanediol (AP), and cysteine (Cys). The alkyl amine HDA was selected because of its availability as a stabilizing ligand in the QD fabrication process

and its optimal chain length with respect to the chain length of plasma membrane lipids. HDA readily reacts with CS_2 to form a DTC, resulting in the characteristic absorbance peak at 260 nm and 300 nm **(Figure 1A)**. This molecule is hereafter referred to as HDA-DTC. QDs capped first with hydrophilic molecules such as Lys can be mixed with an organic phase containing HDA-DTC at different ratios **(Figure 1B)**. We designate these QDs as HDA-Lys-QDs. The addition of different amounts of HDA-DTC molecules to QDs can detrimentally affect the final QD preparation in two ways. First, if the number of HDA-DTC per QD is moderately high, aggregation in the aqueous phase results in a higher background absorbance at high wavelengths due to increased light scattering **(Figure 1C)**. This was quantified as the turbidity index. Additionally, a high coverage of HDA-DTC on QDs induces insoluble aggregates in the aqueous phase, driving particles into the organic phase during the biphasic reaction (Figure 1B). This results in a lower measured absorbance in the aqueous phase at short wavelengths due to a decreased soluble concentration. This was quantified as the normalized aqueous concentration. Useful QD:HDA-DTC ratios would then exhibit a low turbidity index and high normalized aqueous concentration, resulting in a high solubility index. Using these metrics, a 1:10 ratio of QD:HDA-DTC performed better than ratios of either 1:50 or 1:100 (Figure 1C).

Given that Lys-QDs accept HDA-DTC as an additional surface ligand, but increased HDA-DTC results in aggregation, we wanted to more precisely examine the aggregation state of HDA-DTC modified hydrophilic QDs, including those capped with Lys, AP, and Cys (Table 1). We used both dynamic light scattering (DLS) and epi-fluorescence microscopy to quantify the size distribution of the QDs in different buffers that are relevant to biological studies. These include water, a balanced salt solution (phosphate buffered saline, PBS), and a cell medium (Dulbecco's Modified Eagle's Medium, DMEM), some of which included protein additives commonly used with cells: bovine serum albumin (BSA) and fetal bovine serum (FBS). Aqueous buffers affected the aggregation of even the hydrophilic

QDs (Lys-QD, AP-QD, and Cys-QD) in non-intuitive ways. For instance, Cys-QDs did not aggregate in PBS at all, but aggregated extensively in DMEM, even though the pH and ionic strengths of both solutions are approximately the same (Table 1). Additionally, protein additives commonly used in

biological applications prevented aggregation of HDA-DTC modified QDs, however, the potential for this enhancement with BSA or FBS depended on the hydrophilic ligand. Understanding aggregation of these different species of QDs is critical and was used to design experiments for assessing cell and tissue binding.

3.2 Quantification and Analysis of Cell Binding Ability of Lipid-Modified Quantum Dots. In order to examine the affinity of these different hydrophilic ligands, with and without HDA-DTC, towards live cells, we turned to flow cytometry studies where mouse fibroblast cells were incubated with various species of QDs. Binding of both HDA-Lys-QDs and Lys-QDs were dose dependent, however HDA-Lys-QDs were more sensitive to the dose. A concentration of 1 μM led to significant cell binding and was used as a constant QD concentration for other flow cytometry experiments. The cell binding behavior of HDA-Lys-QDs largely matched the behavior of DiD, a common lipophilic dye used to stain cell membranes. While extinction coefficients, quantum yields, and excitation/emission filter characteristics were different between the HDA-Lys-QDs and DiD, HDA-Lys-QD binding to the cell membrane was on the same order of magnitude as DiD binding **(Figure 2A)**. Interestingly, this dose response also depended on the number of freeze-thaw cycles experienced by the QD sample (supplementary Figure 1). Consequently, QDs having the same number of freeze-thaw cycles were used for analysis.

The cell binding of six different species of QDs (3 hydrophilic ligands +/- HDA-DTC) was evaluated using flow cytometry where the enhancement due to the addition of HDA-DTC was calculated. Because the fluorescence of the different species of QDs was slightly different (supplementary Figure 2), the flow cytometry fluorescence was normalized to the fluorescence measured using a cuvette fluorometer. QDs bearing Cys ligands bound to cells with the highest affinity **(~5× greater than the other QD**

species, Figure 2B), however this binding was actually diminished by the addition of HDA-DTC **(Figure 2C)**. QDs bearing Cys ligands contain free sulfhydryl groups that can form disulfide bonds with cell surface proteins containing exposed Cys. This reaction might be inhibited to some extent by the

addition of lipid on the surface of the QD. Both Lys and AP showed lower overall binding (Figure 2B), but statistically significant enhancement of cell binding in response to the addition of the HDA-DTC (Figure 2C). All of the hydrophilic ligands resulted in net negatively charged QDs, but the charge order was the same based on the charge of the hydrophilic ligand itself. Interestingly, enhancement due to the presence of HDA-DTC was linearly proportional to the ζ-potential (Figure 2C). This is noteworthy and indicates that QD surface charge not only regulates solubility, but impacts binding affinity as well.[33] While we do not know how the enhancement would depend on charge for QDs with a net positive charge, generating QDs with charges near zero could increase the enhancement to ~3-fold.

While examining cells labeled with both DiD and QDs, we found that the addition of a 10-fold higher concentration of lipophilic molecule like DiD enhanced the binding of both HDA-AP-QDs and HDA-Cys-QDs and to a lesser extent AP-QD and Cys-QDs **(Figure 3)**. However, it decreased the binding of both Lys-coated QDs. This suggests that lipid carriers might provide a mechanism by which to introduce these mixed surface QDs, however the nature of the hydrophilic ligand must be considered. Given the enhancement of the cell binding ability of HDA-Lys-QD over Lys-QD in buffers without lipid additives, we turned to microscopy to analyze the QD binding to and movement within cells.

Mouse fibroblast cells were incubated with either Lys-QDs or HDA-Lys-QDs, washed, and allowed to spread onto fibronectin-coated cover slips. After the cells spread, TIRF images were taken at < 0.3 s time intervals. Lys-QD treated cells showed very few mobile QDs **(Figure 4A and supplemental Video 1)**. These static particles were most likely QDs that are nonspecifically attached to the glass. In contrast, while there was also some nonspecific attachment of HDA-Lys-QDs to the glass, there were clear instances of mobile particles on the ventral membrane in HDA-Lys-QD-treated cells **(Figure 4A and supplemental Video 2)**. The length scale of motion (~0.5 μm) of small particles over the sampling time interval (~0.6 s) yields a diffusion coefficient of ~0.4 $\mu m^2/s$, which is similar in magnitude to

membrane-tethered protein diffusion. Both Lys-QDs and HDA-Lys-QDs were readily internalized, accumulating in vesicles docked at the ventral membrane as visible by TIRF. Both vesicle movement, a

long timescale event, and individual QD diffusion, a short timescale event, impact the overall movement of punctae in images. This movement can be quantified by calculating a temporal autocorrelation value, which compares image intensity pixel-by-pixel over different time lags. Slower moving particles result in temporal autocorrelation curves that decrease at longer time lags. Temporal autocorrelation functions were dramatically different between Lys-QDs and HDA-Lys-QDs in both the cell body and periphery (Figure 4B and C). Additionally, a model for the autocorrelation function that incorporates two distinct timescales for diffusion from two different populations of vesicles (~100 s) and single QDs (~0.1 s) did not fit the Lys-QD data (Figure 4B). Visual inspection of the timelapses of QD movement and examination of the temporal autocorrelation functions leads us to believe that adding HDA-DTC to QDs containing hydrophilic ligands facilitates QD attachment to and diffusion within the plane of the membrane.

3.3 Quantification and Analysis of Tissue Binding Ability of Lipid-Modified Quantum Dots. Given that HDA-DTC enhances the cell binding of some, but not all, hydrophilic QDs, we tested if similar behavior would be observed in animal tissues. We hypothesized that HDA-DTC would enhance the localization of QDs to plasma membranes and to lipid-rich cytoplasmic organelles in thin frozen tissue sections. Consequently, we prepared 3 μm thick frozen tissue sections from canine liver, incubated these samples with QDs, Alexa Fluor 488-labeled phalloidin, and DAPI, and evaluated QD binding quantitatively and qualitatively. Tremendous similarity existed between the trends in the QD affinity to cells and tissues **(compare Figure 2B and Figure 5B)**, even though cell binding as measured by flow cytometry did not show the same level of statistical significance. Furthermore, some species of QDs demonstrated enhanced binding to the borders of cells in the hepatic parenchyma using a one sample *t* test **($p = 0.05$, Figure 5C)**. QDs bound peripherally along the cytoplasmic actin network near basal

cytoplasmic margins of hepatocytes, the location of the cell membrane of hepatocytes, with differences in cell border binding among QD constructs. Both Cys- and Lys-coated QDs show enhanced binding when HDA-DTC is added, with the addition of HDA-DTC resulting in a statistically significant

difference in cell border binding for Cys-QDs **(Figure 5A and C)**. On the other hand, AP-coated QDs bound cells well, but the addition of HDA-DTC reduced the preferential binding to the cell border. The subcellular distribution of QDs supports the hypothesis that the QDs with various ligands differentially bind to some components of the plasma membrane and cytoplasm.

Differential binding was not, however, limited to the plasma membrane and cytoplasm. Hepatic cords are composed of hepatocytes arranged with stringent apical-basolateral polarization that reflects some of the physiologic function of the liver, namely the uptake, processing, metabolism, transport, and excretion of many metabolic and toxic molecules, as well as the production of bile. The apical membrane of hepatocytes lining bile canaliculi is a site of intense secretory transport involved in the production of bile, a secretion of hepatocytes that functions to some extent as a surfactant, emulsifying lipids in the digestive tract. None of the QD constructs co-localize with the F-actin-dense microvilli of the apical hepatic membrane lining bile canaliculi between hepatocytes (Figure 5A). We theorize that differences in QD binding between the apical and basolateral membranes of hepatocytes are due to compositional differences in these membrane domains. Additionally, all species of QDs and HDA-QDs demonstrated multifocal, variably intense perinuclear binding of the nuclei of some hepatocytes **(Figure 5D)**. We theorize that the perinuclear capping may be related to the presence of intracytoplasmic membrane-rich regions, such as Golgi apparatus and other organelles, or, possibly, to positively charged molecules attracted to the negative charge of DNA, or to the negative charge of DNA itself.

Having observed this spatial inhomogeneity of QD binding among membrane components with different functions in hepatocytes, we examined QD-labeling of a variety of cell types forming complex architectural structures in the frozen liver sections. The increased affinity of binding by Cys-QDs and HDA-Cys-QDs as compared with other species is evident, including HDA-Lys-QD as shown in Fig 6. Binding of QD constructs to the epithelial cells lining bile ductules was usually limited to mild, granular

fluorescence of the cytoplasm and faint perinuclear (apical) binding, but for some constructs there was variability of binding to epithelia, even within sections (Fig 6). Kupffer cells lining hepatic sinusoids often demonstrated moderately intense perinuclear binding of all QD constructs and no appearance of

differential plasma membrane versus cytoplasmic binding. Small numbers of endothelial cells have mild perinuclear binding. Cellular and fibrous components of the portal region demonstrated faint binding of HDA-Lys-QD and much stronger binding of Cys-QD, HDA-Cys-QD **(Figure 6)**. The endothelial lining of the portal venules bind Cys-QD and HDA-Cys-QDs intensely, with minimal binding of HDA-Lys-QD.

4. Conclusion

This work demonstrated a number of important findings with respect to the generation of biocompatible QDs. First, we showed that surface ligands on QDs can dramatically affect solubility in different aqueous buffers. This is of vital importance in designing a biosensor as many solvents are not compatible with cells and tissues. Second, the charge and hydrophobicity of surface ligands covering the QD can tune the degree of cell and tissue binding. We expect this phenomenon to regulate other targeting approaches using either hydrophobic alpha-helix forming peptides[34] or specific targeting peptides.[35] Finally, QDs lacking specific targeting mechanisms such as antibody-antigen or ligand-receptor interactions are able to spatially localize to both subcellular and anatomical structures. Tuning surface charge and hydrophobicity is expected to allow development of new tools for histology that can complement techniques such as immunohistopathology. Consequently, designing biosensors with targeting characteristics does not solely rest with identifying a specific receptor-ligand pair, but rather also depends strongly on nonspecific interactions that originate from the nanoparticle and, importantly, that can be controlled during their synthesis. Tuning these nonspecific interactions between QDs and cells to optimize or reduce cell binding might hold more promise for cell targeting or avoidance than previously thought.

Acknowledgements

This work was supported by startup funds from Iowa State University, including the Office of Biotechnology. We thank Shawn Rigby in the flow cytometry facility for analyzing samples and

Jennifer Groeltz-Thrush in the Iowa State University Veterinary Histopathology Laboratory for cutting frozen sections.

References

[1] V.V. Breus, C.D. Heyes, K. Tron, G.U. Nienhaus, Zwitterionic Biocompatible Quantum Dots for Wide pH Stability and Weak Nonspecific Binding to Cells, Acs Nano 3 (2009) 2573-2580.
[2] K.-i. Hanaki, A. Momo, T. Oku, A. Komoto, S. Maenosono, Y. Yamaguchi, K. Yamamoto, Semiconductor quantum dot/albumin complex is a long-life and highly photostable endosome marker, Biochem. Biophys. Res. Commun. 302 (2003) 496-501.
[3] H. Mattoussi, J.M. Mauro, E.R. Goldman, G.P. Anderson, V.C. Sundar, F.V. Mikulec, M.G. Bawendi, Self-Assembly of CdSe−ZnS Quantum Dot Bioconjugates Using an Engineered Recombinant Protein, J. Am. Chem. Soc. 122 (2000) 12142-12150.
[4] S. Pathak, S.-K. Choi, N. Arnheim, M.E. Thompson, Hydroxylated Quantum Dots as Luminescent Probes for in Situ Hybridization, J. Am. Chem. Soc. 123 (2001) 4103-4104.
[5] C. Querner, P. Reiss, J. Bleuse, A. Pron, Chelating Ligands for Nanocrystals' Surface Functionalization, J. Am. Chem. Soc. 126 (2004) 11574-11582.
[6] H. Tetsuka, T. Ebina, F. Mizukami, Highly Luminescent Flexible Quantum Dot-Clay Films, Adv. Mater. 20 (2008) 3039-3043.
[7] X. Hu, X. Gao, Silica−Polymer Dual Layer-Encapsulated Quantum Dots with Remarkable Stability, Acs Nano 4 (2010) 6080-6086.
[8] U. Resch-Genger, M. Grabolle, S. Cavaliere-Jaricot, R. Nitschke, T. Nann, Quantum dots versus organic dyes as fluorescent labels, Nat. Meth. 5 (2008) 763-775.
[9] X. Wu, H. Liu, J. Liu, K.N. Haley, J.A. Treadway, J.P. Larson, N. Ge, F. Peale, M.P. Bruchez, Immunofluorescent labeling of cancer marker Her2 and other cellular targets with semiconductor quantum dots, Nat. Biotech. 21 (2003) 41-46.
[10] W.W. Yu, E. Chang, J.C. Falkner, J. Zhang, A.M. Al-Somali, C.M. Sayes, J. Johns, R. Drezek, V.L. Colvin, Forming Biocompatible and Nonaggregated Nanocrystals in Water Using Amphiphilic Polymers, J. Am. Chem. Soc. 129 (2007) 2871-2879.
[11] W.J. Parak, D. Gerion, T. Pellegrino, D. Zanchet, C. Micheel, S.C. Williams, R. Boudreau, M.A.L. Gros, C.A. Larabell, A.P. Alivisatos, Biological applications of colloidal nanocrystals, Nanotechnology 14 (2003) R15-R27.
[12] S. Doose, J.M. Tsay, F. Pinaud, S. Weiss, Comparison of Photophysical and Colloidal Properties of Biocompatible Semiconductor Nanocrystals Using Fluorescence Correlation Spectroscopy, Anal. Chem. 77 (2005) 2235-2242.
[13] T. Pellegrino, L. Manna, S. Kudera, T. Liedl, D. Koktysh, A.L. Rogach, S. Keller, J. Rädler, G. Natile, W.J. Parak, Hydrophobic Nanocrystals Coated with an Amphiphilic Polymer Shell: A General Route to Water Soluble Nanocrystals, Nano Lett. 4 (2004) 703-707.
[14] Y. Zhang, A.M. Schnoes, A.R. Clapp, Dithiocarbamates as Capping Ligands for Water-Soluble Quantum Dots, ACS Appl. Mater. Interfaces 2 (2010) 3384-3395.
[15] F. Sabeh, R. Shimizu-Hirota, S.J. Weiss, Protease-dependent versus -independent cancer cell invasion programs: three-dimensional amoeboid movement revisited, J. Cell Biol. 185 (2009) 11 -19.

[16] K. Wolf, Y.I. Wu, Y. Liu, J. Geiger, E. Tam, C. Overall, M.S. Stack, P. Friedl, Multi-step pericellular proteolysis controls the transition from individual to collective cancer cell invasion, Nat. Cell Biol. 9 (2007) 893-904.
[17] M.S. Wolfe, Intramembrane-cleaving Proteases, J. Biol. Chem. 284 (2009) 13969 -13973.

[18] N.P. Mahajan, D. Corinne Harrison-Shostak, J. Michaux, B. Herman, Novel mutant green fluorescent protein protease substrates reveal the activation of specific caspases during apoptosis, Chem. Biol. 6 (1999) 401-409.
[19] U. Neumann, H. Kubota, K. Frei, V. Ganu, D. Leppert, Characterization of Mca-Lys-Pro-Leu-Gly-Leu-Dpa-Ala-Arg-NH2, a fluorogenic substrate with increased specificity constants for collagenases and tumor necrosis factor converting enzyme, Anal. Chem. 328 (2004) 166-173.
[20] J. Zhang, R.E. Campbell, A.Y. Ting, R.Y. Tsien, Creating new fluorescent probes for cell biology, Nat. Rev. Mol. Cell Biol. 3 (2002) 906-918.
[21] J. Lin, Z. Zhang, J. Yang, S. Zeng, B.-F. Liu, Q. Luo, Real-time detection of caspase-2 activation in a single living HeLa cell during cisplatin-induced apoptosis, J. Biomed. Opt. 11 (2006) 024011.
[22] J. Lin, Z. Zhang, S. Zeng, S. Zhou, B.-F. Liu, Q. Liu, J. Yang, Q. Luo, TRAIL-induced apoptosis proceeding from caspase-3-dependent and -independent pathways in distinct HeLa cells, Biochem. Biophys. Res. Commun. 346 (2006) 1136-1141.
[23] M. Ouyang, S. Lu, X.-Y. Li, J. Xu, J. Seong, B.N.G. Giepmans, J.Y.-J. Shyy, S.J. Weiss, Y. Wang, Visualization of Polarized Membrane Type 1 Matrix Metalloproteinase Activity in Live Cells by Fluorescence Resonance Energy Transfer Imaging, J. Biol. Chem. 283 (2008) 17740 -17748.
[24] J. Yang, Z. Zhang, J. Lin, J. Lu, B.-f. Liu, S. Zeng, Q. Luo, Detection of MMP activity in living cells by a genetically encoded surface-displayed FRET sensor, Biochim. Biophys. Acta, Mol. Cell. Res. 1773 (2007) 400-407.
[25] H. Arya, Z. Kaul, R. Wadhwa, K. Taira, T. Hirano, S.C. Kaul, Quantum Dots in Bio-imaging: Revolution by the Small, Biochem. and Biophys. Res. Commun. 329 (2005) 1173-1177.
[26] X. Gao, L. Yang, J.A. Petros, F.F. Marshall, J.W. Simons, S. Nie, In Vivo Molecular and Cellular Imaging with Quantum Dots, Curr. Opin. Biotechnol. 16 (2005) 63-72.
[27] B.N.G. Giepmans, The Fluorescent Toolbox for Assessing Protein Location and Function, Science 312 (2006) 217-224.
[28] E.R. Goldman, E.D. Balighian, H. Mattoussi, M.K. Kuno, J.M. Mauro, P.T. Tran, G.P. Anderson, Avidin: A Natural Bridge for Quantum Dot-Antibody Conjugates, J. Am. Chem. Soc. 124 (2002) 6378-6382.
[29] L. Groc, M. Heine, L. Cognet, K. Brickley, F.A. Stephenson, B. Lounis, D. Choquet, Differential activity-dependent regulation of the lateral mobilities of AMPA and NMDA receptors, Nat. Neurosci. 7 (2004) 695-696.
[30] M. Howarth, K. Takao, Y. Hayashi, A.Y. Ting, Targeting quantum dots to surface proteins in living cells with biotin ligase, PNAS 102 (2005) 7583 -7588.
[31] M.J. Murcia, D.E. Minner, G.-M. Mustata, K. Ritchie, C.A. Naumann, Design of Quantum Dot-Conjugated Lipids for Long-Term, High-Speed Tracking Experiments on Cell Surfaces, J. Am. Chem. Soc. 130 (2008) 15054–15062.
[32] D.L. Kolin, P.W. Wiseman, Advances in image correlation spectroscopy: Measuring number densities, aggregation states, and dynamics of fluorescently labeled macromolecules in cells, Cell Biochem. Biophys. 49 (2007) 141-164.
[33] J. Park, J. Nam, N. Won, H. Jin, S. Jung, S.H. Cho, S. Kim, Compact and Stable Quantum Dots with Positive, Negative, or Zwitterionic Surface: Specific Cell Interactions and Non-Specific Adsorptions by the Surface Charges, Adv. Funct. Mater. 21 (2011) 1558-1566.
[34] O.A. Andreev, A.D. Dupuy, M. Segala, S. Sandugu, D.A. Serra, C.O. Chichester, D.M. Engelman, Y.K. Reshetnyak, Mechanism and uses of a membrane peptide that targets tumors and other acidic tissues in vivo, Proc. Natl. Acad. Sci. U. S. A. 104 (2007) 7893-7898.

[35] K.A. Kelly, N. Bardeesy, R. Anbazhagan, S. Gurumurthy, J. Berger, H. Alencar, R.A. DePinho, U. Mahmood, R. Weissleder, Targeted nanoparticles for imaging incipient pancreatic ductal adenocarcinoma, Plos Medicine 5 (2008) 657-668.

Figures

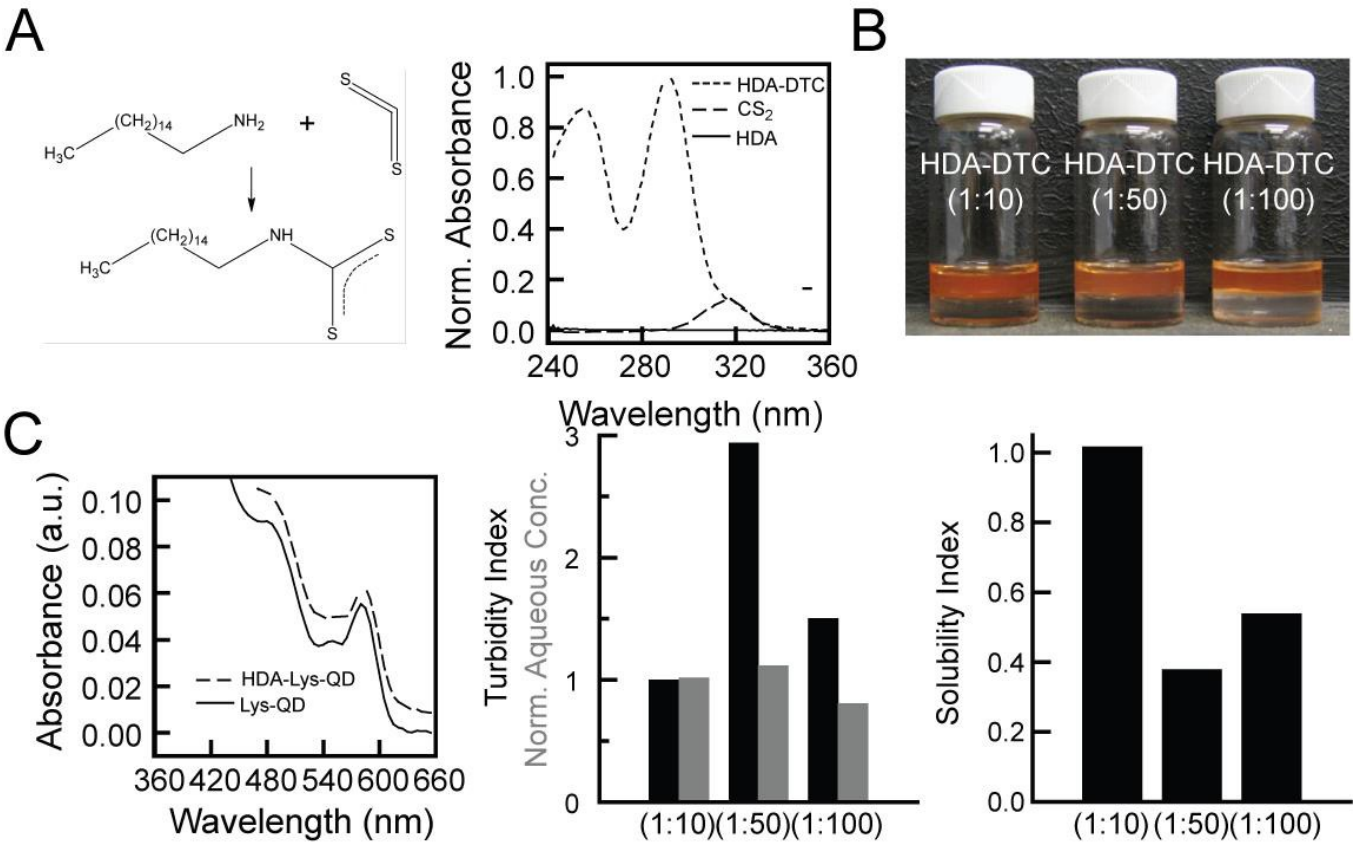

Figure 1. Synthesis of soluble lipid-tethered QDs using partial ligand exchange: A. Left: CS_2 reacts with HDA at the primary amine to form a DTC-containing hydrophobic molecule. Right: Absorbance spectra are shown for products and reactants. B. Images show the two phase system after partial ligand exchange with HDA-DTC. The aqueous phase (red) is on top and the organic phase (clear or cloudy) is on bottom. Different QD:HDA-DTC ratios are shown. C. Left: Absorbance spectra of HDA-Lys-QDs (1:10 QD:HDA-DTC ratio) and Lys-QDs (before partial exchange with HDA-DTC). Turbidity index (middle), normalized QD concentration (middle), and solubility index (turbidity index/normalized QD concentration, right) was calculated for HDA-Lys-QDs in aqueous solution with different QD:HDA-

DTC ratios.

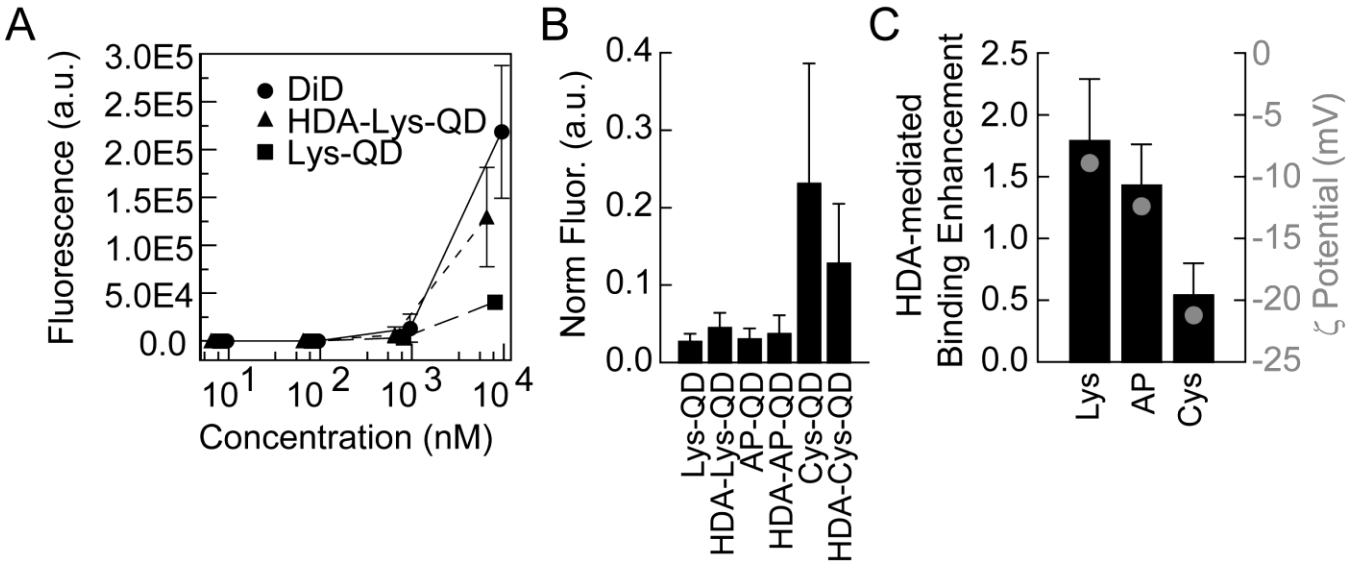

Figure 2. Lipid-tethered QDs show differential cell binding: A. Mean background subtracted fluorescence from flow cytometry is shown as a function of fluorescent probe dose. Cells were incubated for 30 minutes with DiD (a lipid dye), HDA-Lys-QDs, or Lys-QDs at the given concentrations (N = 3). B. Normalized fluorescence from flow cytometry after cells were incubated with 1 μM QD for 30 minutes. Normalized fluorescence was calculated as the mean background subtracted fluorescence from flow cytometry is divided by the background subtracted fluorescence of the same concentration of QD as measured by a cuvette fluorometer (N > 5). C. Black bars: The fluorescence signal from flow cytometry of the HDA-derivative divided by the fluorescence signal from QD before HDA exchange (N > 5). Gray dots: The particle charge for Lys (N = 2), AP (N = 1), and Cys (N = 3). All error bars represent 95% confidence intervals.

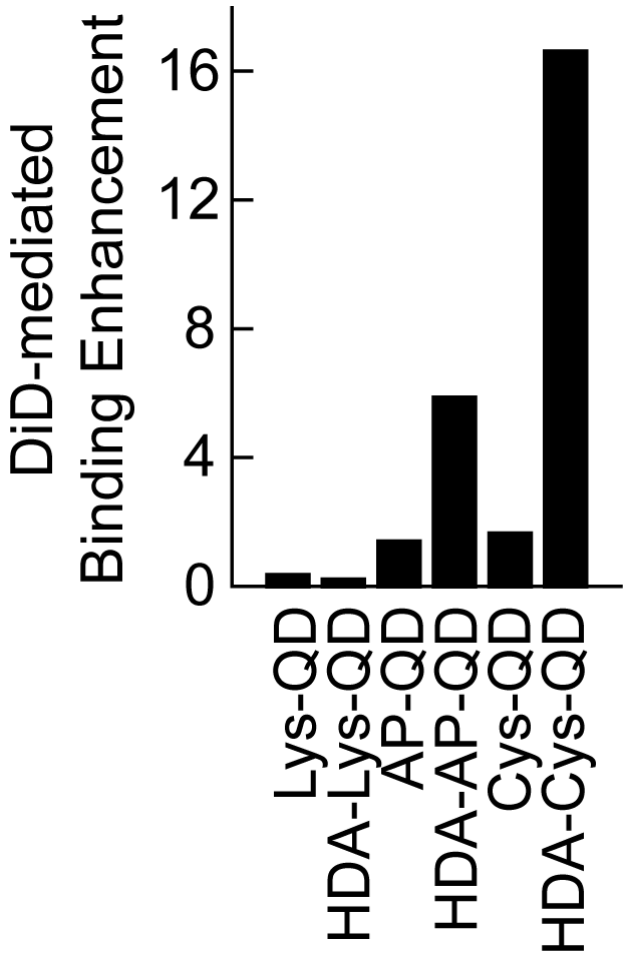

Figure 3. DiD enhances the cell binding of lipid-tethered QDs: DiD-mediated binding enhancement was measured using flow cytometry. Mean background subtracted fluorescence of cells incubated with 1 μM QD and 10 μM DiD was divided by the mean background subtracted fluorescence of cells incubated with 1 μM QD only.

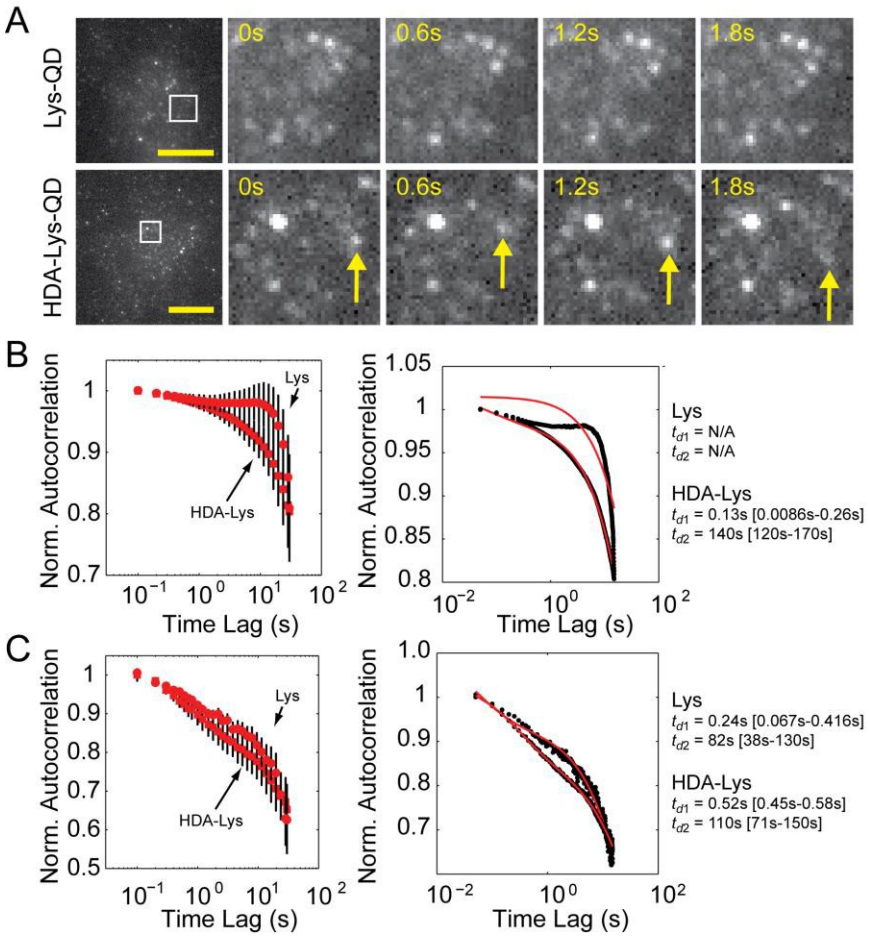

Figure 4. Lipid-tethered QDs show differential mobility in the cell membrane: A. Cells were incubated with 0.3-1 μM Lys-QD or HDA-Lys-QD before imaging using TIRF. The whole cell is shown on the left and a montage of images take 600 ms apart is shown to the right. The arrow marks a mobile QD in the cell membrane. The scale bar is 10 μm. B. TICS was used to construct normalized autocorrelation as a function of time lag for particles in the cell body. Left: Average normalized autocorrelation for multiple cells over three days for both Lys-QDs (N = 20) and HDA-Lys-QDs (N =

14) is shown with error bars representing 95% confidence intervals. Right: Model of 2D diffusion of two different populations (red) is shown with the data (black). Characteristic diffusion times are presented to the right with 95% confidence intervals included in the brackets. C. TICS was used to

construct normalized autocorrelation as a function of time lag for particles in the lamellipodia of cells. This was done for three regions in a cell for multiple cells over three days for both Lys-QDs (N = 20) and HDA-Lys-QDs (N = 14). Measurements and diffusion times were presented as in B.

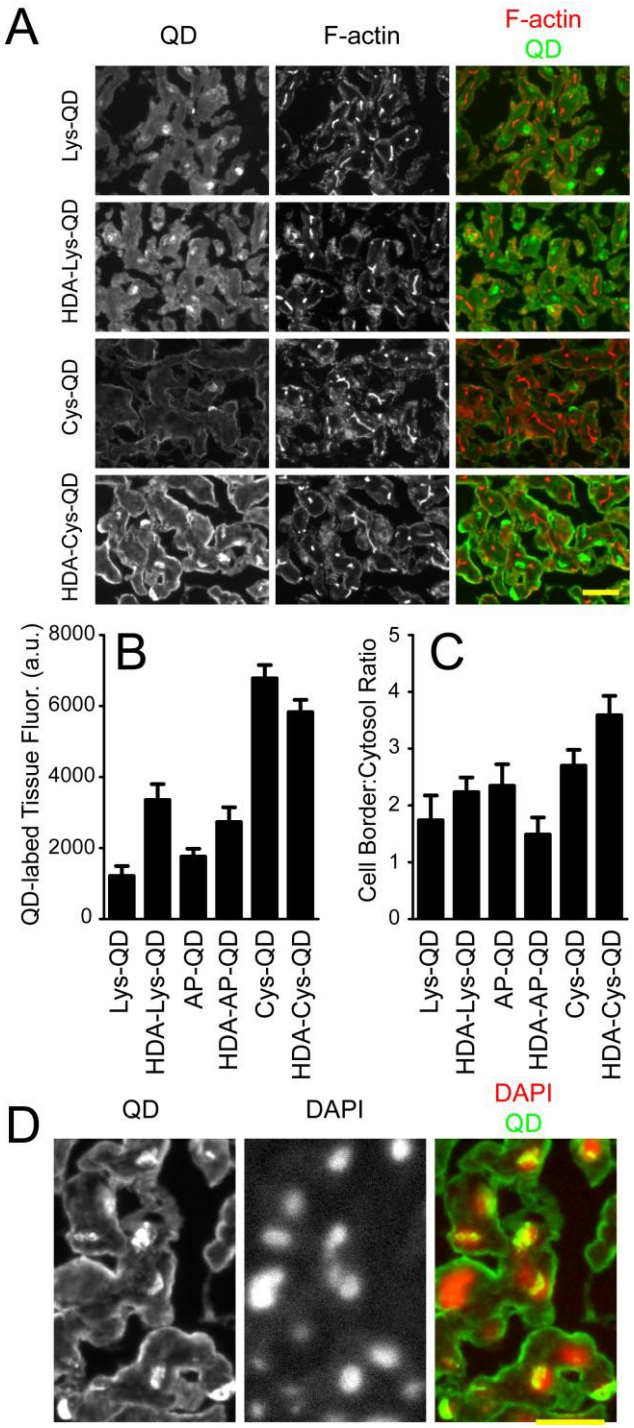

Figure 5. Lipid-tethered QDs show differential binding to liver tissue: A. Liver tissue frozen sections were incubated with 1 μM QD and phalloidin for 30 minutes. Homogeneous fields were imaged using low magnification widefield fluorescence microscopy. HDA-derivatives and their

corresponding control QD before HDA exchange were scaled the same. Left: QD signal is shown. Middle: Phalloidin (F-actin) signal is shown. Right: Overlay of QD signal (green) and F-actin signal (red). B. Mean field background subtracted fluorescence was quantified for the different QDs ($N > 10$

fields). This fluorescence was not normalized by intrinsic QD fluorescence as in figure 2. C. Cortical cell membrane fluorescence divided by cytosolic fluorescence was quantified for the different QDs (N > 10). D. Cells prepared as in A Left: HDA-Cys-QD signal is shown. Middle: DAPI signal is shown. Right: Overlay of QD signal (green) and DAPI signal (red). All error bars represent 95% confidence intervals. Scale bars are 20 μm.

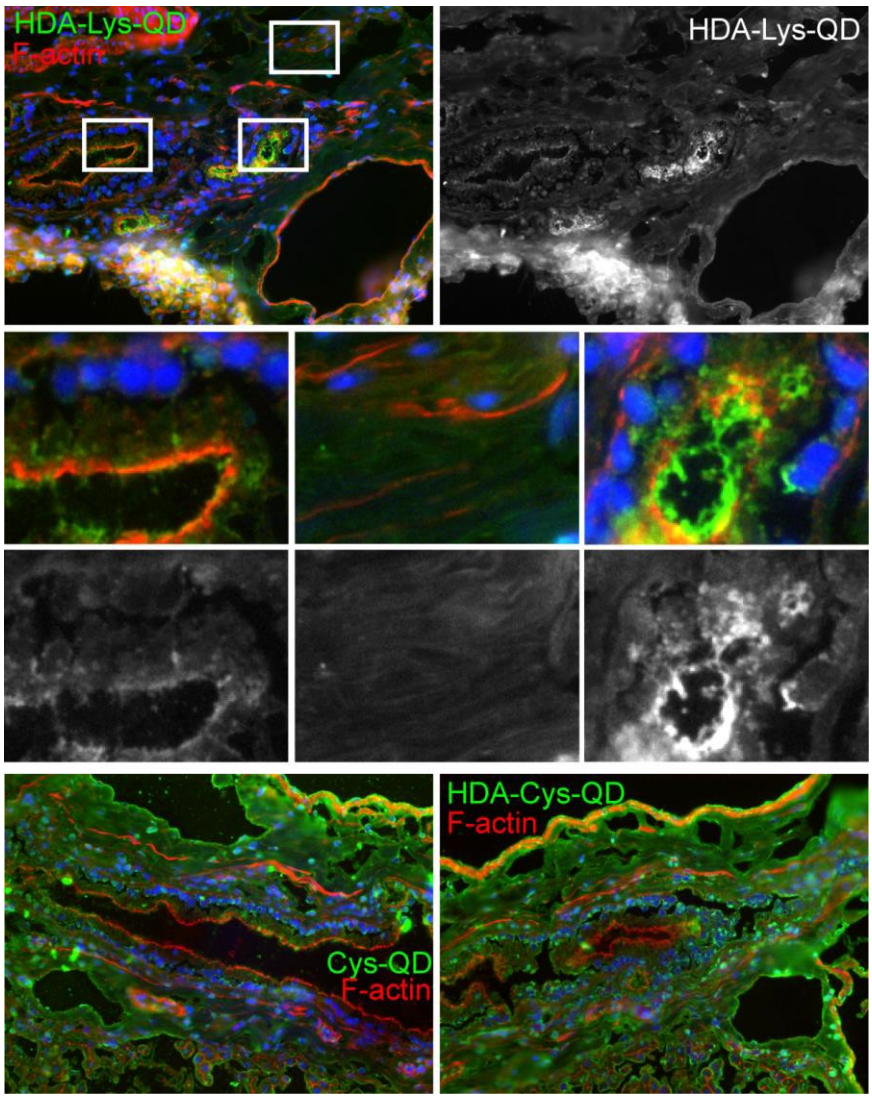

Figure 6. QDs localize to distinct regions in liver tissue: Top: Liver tissue section stained with HDA-Lys-QD (green), phalloidin (actin) and DAPI (blue) as in Figure 5. Middle: Enlarged regions showing epithelium of a collecting bile ductule (left), interstitium of the portal region (middle) and a small bile ductule (right). Bottom: Liver tissue section stained with Cys-QD (green, left) or HDA-Cys-QD (green, right), phalloidin (actin) and DAPI (blue) as in Figure 5.

Tables

Table 1. Aggregation characteristics for different mixed surface QDs: Dynamic light scattering (DLS) and epi-fluorescence microscopy (EFM) at low magnification (10×, with a pixel size of 645 nm) was used to characterize the aggregation of differently coated QDs in common buffers compatible with cells as well as the stock solvent, water. Average size from DLS is reported in nanometers and intensity standard deviation fold over background noise from EFM is reported in parentheses.

	Lys	HDA-Lys	Cys	HDA-Cys	AP	HDA-AP
H_2O	6.9	7.6 (3.9)	5.6	7.6	16	21
PBS	5.1	24 (150)	7.8	11	120[a]	35
PBS+FBS	n.d.	n.d.	6.1	6.4	n.d.	n.d.
PBS+BSA	n.d.	n.d.	10	15	n.d.	n.d.
DMEM	6.7	22 (65)	220[a]	27	82[a]	900
DMEM+FBS	n.d.	n.d. (3.5)	n.d.	n.d.	n.d.	n.d.
DMEM+BSA	4.0	3.9 (4.4)	44	54[a]	15	23

[a] indicates double peaks in the particle size distributions based on number

n.d. indicates conditions that were not used

Supporting Information

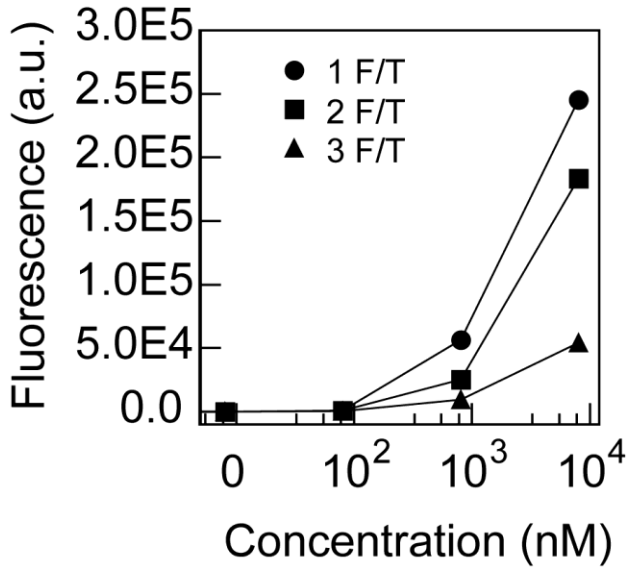

Supplementary Figure 1. The number of freeze-thaw cycles affects QD binding to cells: Cell binding was measured with flow cytometry as in figure 2 and 3. The background subtracted mean fluorescence of cells treated with various doses of HDA-Lys-QD for 30 minutes is shown after 1-3 freeze-thaw cycles.

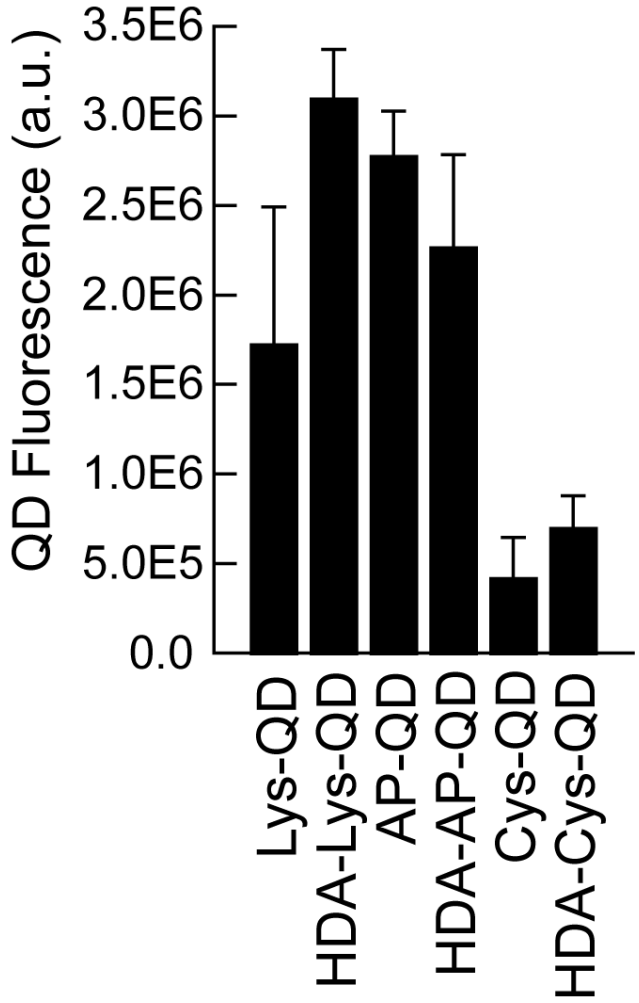

Supplementary Figure 2. Ligand surface affects QD fluorescence: Fluorescence was measured using a cuvette fluorometer the same day flow cytometry was conducted. Mean background substracted fluorescence is shown for all six ligand coats ($N > 5$). Error bars represent 95% confidence intervals.

Supplementary Video 1. TIRF imaging of Lys-QDs on cells: Images were taken every 600 ms for 1 minute. The frame rate is 15 frames per second, resulting in 9× actual speed. This movie corresponds to the top row of images in figure 4A.

Supplementary Video 1. TIRF imaging of HDA-Lys-QDs on cells: Images were taken every 600 ms for 1 minute. The frame rate is 15 frames per second, resulting in 9× actual speed. This movie corresponds to the bottom row of images in figure 4A.